

# Plasmonic response of a nanorod in the vicinity of a metallic surface: local approach with analytical solution

I. M. Vasilevskiy<sup>1</sup> and N. M. R. Peres<sup>1,2</sup>

<sup>1</sup>University of Minho, Department of Physics and Center of Physics and Quantalab, 4710-057 Braga, Portugal

<sup>2</sup>International Iberian Nanotechnology Laboratory (INL), Avenida Mestre José Veiga, 4715-330 Braga, Portugal

**Abstract.** In this paper we present an analytical solution for the eigenmodes and corresponding electric fields of a composite system made of a nanorod in the vicinity of a plasmonic semi-infinite metallic system. To be specific, we choose Silver as the material for both the nanorod and the semi-infinite metal. The system is composed of two sub-systems with different symmetries: the rod has axial symmetry, while the interface has a rectangular one. Using a boundary integral method, proposed by Eyges, we are able to compute analytically the integrals that sew together the two systems. In the end, the problem is reduced to a one of linear algebra, where all the terms in the system are known analytically. For large distances between the rod and the planar surface, only a few of those integrals are needed and a full analytical solution can be obtained. Our results are important to benchmark other numerical approaches and represent a starting point in the discussion of systems composed of nanorods and two-dimensional materials.

## 1. Introduction

Nanophotonics, involving plasmonic components, is nowadays at the heart of many different technologies, such as gas sensors, efficient solar cells, highly sensitive photodetectors and photonic devices [1]. The ability to confine electromagnetic radiation, spanning the spectral range from the THz to the UV, into tiny geometric spaces is one of the victories of modern nanophotonics. From the THz to the mid-IR, graphene can work as a plasmonic material [2, 3, 4, 5], showing outstanding confinement of electromagnetic radiation down to one atom thickness. On the other hand, more conventional materials such as Silver, Gold, and Copper cover the spectral range from the near-IR to the UV, allowing strong electromagnetic confinement in a region not accessible to graphene plasmons. The large degree of electromagnetic field enhancement is achieved in gaps between two metallic structures, spheres or cubes, and between spheres, infinite/semi-infinite rods [6], cubes and a metallic/conductive flat interface.

Several mechanisms concerning plasmonics can be used to efficiently attain light trapping. In the near-field regime, the confinement of electromagnetic waves due to metallic nanostructures leads to localized surface plasmons (LSP). The same nanostructures can also act as launchers of propagation surface plasmon polaritons (SPP) when they are near a semi-infinite planar metallic interface. In plasmon cavity mode there is generation of standing waves and the originated field is independent of the incident light polarization [7]. Another approach to enhance absorption is to focus the incident light beam to the desired location. Metasurfaces are thin flat structures able to change phase, amplitude and polarization of the incident waves [8], favoring the formation of incident wavefronts with specific characteristics. These two-dimensional metamaterials are used for engineering of diverse flat optical devices, such as flat lenses, mirrors, absorbers and anti-reflection layers, namely for the production of solar cells [9].

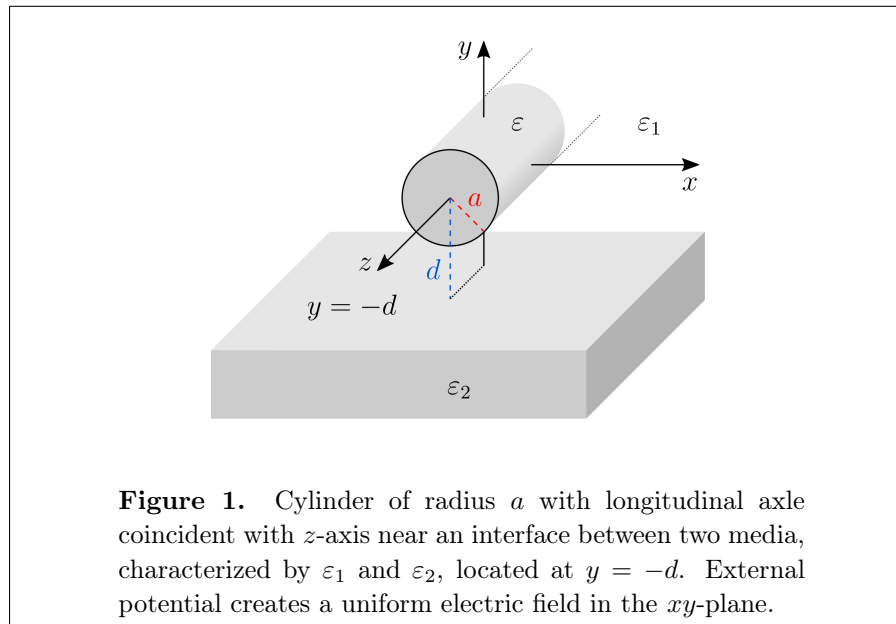
The position of the plasmonic resonance depends on many variables: type of plasmonic material, size and shape of the nanoparticle/rod and dielectric environment. All these possibilities give us a certain degree of freedom to tailor the position of the plasmonic resonance at will. The calculation of the plasmonic resonance is straightforward in simple geometries, on condition that retardation effects are ignored. If the system possesses a high degree of symmetry, such as isolated spheres, rods, toroids, and even combinations of these in certain cases, the analytical calculation of the eigenfrequencies is possible. On the other hand, the integration of two plasmonic systems of different symmetries poses considerable

analytical difficulties because it is not an easy task to match the two disparate symmetries together.

Methods for solving plasmonic problems are abundant, most of them relying on the numerical solution of Maxwell's equations both in time and frequency domains. This approach is nowadays integrated into several commercial software packages. However, it is still important to find analytical solutions to the class of problems we are considering in this paper, allowing to benchmark the numerical methods. Also, analytical solutions frequently put in evidence physical details that may be buried in numerical simulations. In addition to the calculation of the eigenmodes and the fields, other relevant properties of the plasmonic particles and rods, such as their polarizability, are important to extract analytically [10]. The extension of the analytical approach to plasmonic systems composed of metallic nanoparticles/nanorods and two-dimensional materials are also of interest.

As already noted, theoretical studies of polarizability and field enhancement in cylindrical configurations can be obtained from both analytical [11, 12] and numerical [13] methods, being of substantial interest due to diverse physics and engineering applications, such as in the field of plasmonics. The most common recipe for electrostatic problems consists in solving Poisson's equation in differential form. There is, however, a long history of integral method approach to electrostatics, dating back to the first half of the last century [14, 15]. Such methods are very convenient for numerical implementation, as the problem can be transformed into the solution of an exercise in linear algebra. Yet, following this approach there are not many known analytical solutions. In this paper, we present one such solution, where we match together two systems with different symmetries through an integral method: the system in question is a nanorod in proximity of a metallic semi-infinite plane, both of them characterized by a realistic finite dielectric function.

This paper is organized as follows: in Sec. 2 we determine the analytical eigenfrequencies of a nanorod in the proximity of a flat and semi-infinite imperfect metal using the bipolar system of coordinates. Sec. 3 is dedicated to the derivation of the full electrostatic Green's function (actually a tensor) for the rod plus the metallic half-space. In Sec. 4 the determination of the fields follows from the integral method of Eyges, and as a byproduct, the polarizability tensor is determined. In Sec. 5 we give our conclusions and outlook.



## 2. Plasmon modes in cylinder near an infinite flat interface

Consider the following electrostatic problem: given an external electric field, originated from a known electrostatic potential, acting on an infinitely long cylindrical nanorod in the vicinity of a dielectric/metallic interface (Fig. 1), the aim is to find the total potential everywhere in space. This problem can be reduced to a two-dimensional one in the  $xy$ -plane, as the structure and fields are considered invariant under translation along the  $z$ -axis.

The induced field between the cylinder and the interface can be much stronger than the external one if the surface plasmon modes are efficiently excited. These oscillation modes are concentrated near the interface between two different media and their excitation frequency is related to the classical plasma frequency  $\omega_p$  according to the geometry of the system. Solving the Laplace's equation with the appropriate boundary conditions (BC) allows one to determine the desired excitation frequencies.

### 2.1. Eigenfrequencies: the electrostatic limit case

Consider first a system of two infinitely long cylinders of radius  $a$ , as it is shown by Fig. 2. For this geometry the use of bipolar coordinates  $(\mu, \eta)$  is very well suited [16], and as one will see later, it allows a simple transition to the configuration from Fig. 1. If in the Cartesian coordinates the foci  $F_-$  and  $F_+$  are respectively located at  $(0, -u)$  and  $(0, u)$ , the

two systems will be related by:

$$x = \frac{u \sin \eta}{\cosh \mu - \cos \eta}, \quad y = \frac{u \sinh \mu}{\cosh \mu - \cos \eta}, \quad (1)$$

where  $-\infty < \mu < +\infty$  and  $0 \leq \eta < 2\pi$ . The diagonal metric tensor components are equal, thus leaving the Cartesian form of the Laplace's equation for the electric potentials unchanged:

$$\nabla^2 \varphi^{(i)} = \frac{(\cosh \mu - \cos \eta)^2}{u^2} \left( \frac{\partial^2}{\partial \mu^2} + \frac{\partial^2}{\partial \eta^2} \right) \varphi^{(i)} = 0, \quad i = 1, 2, 3. \quad (2)$$

The isosurfaces  $-\mu_-$  and  $\mu_+$  coincide with the circular boundaries of the cylinders characterized by  $\varepsilon_2$  and  $\varepsilon$  respectively, so the following BC are satisfied:

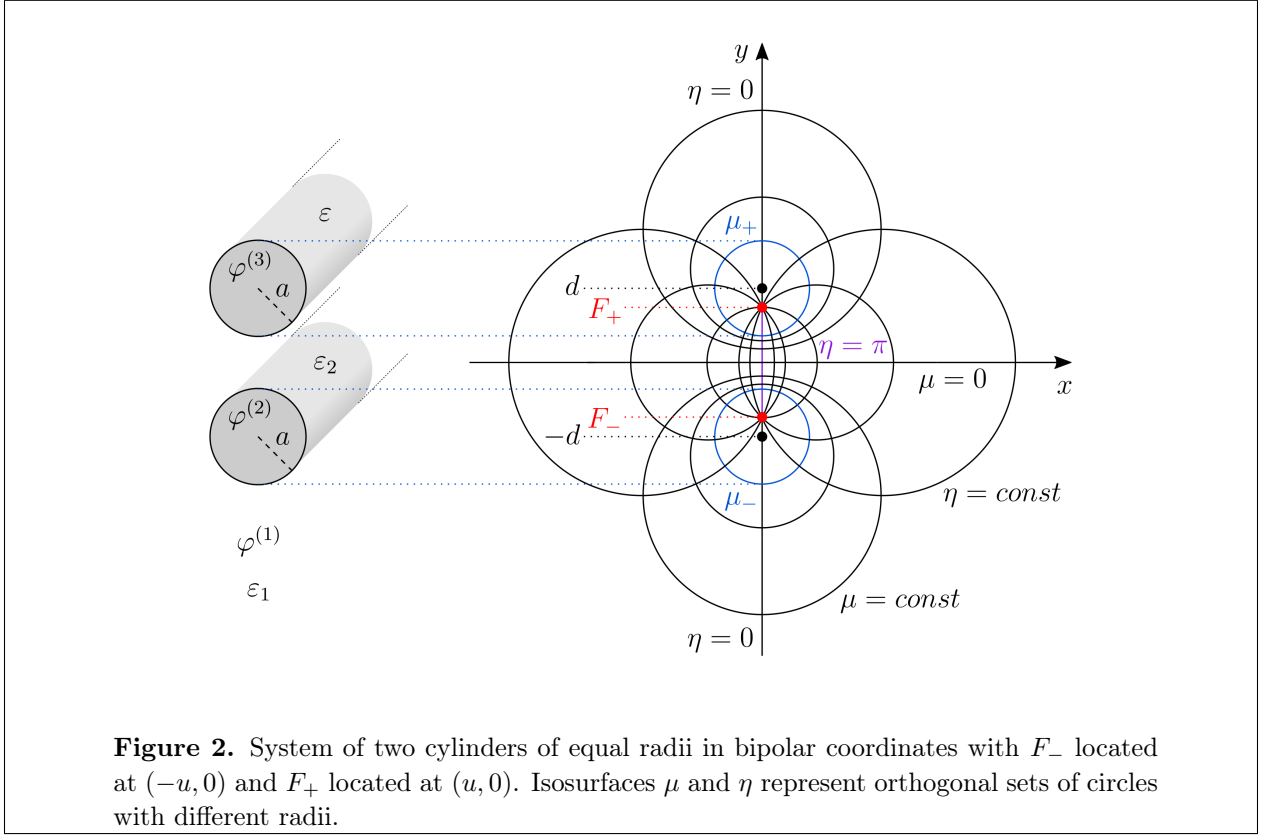
$$\varphi^{(1)}|_{-\mu_-} = \varphi^{(2)}|_{-\mu_-}, \quad (3a)$$

$$\varphi^{(1)}|_{\mu_+} = \varphi^{(3)}|_{\mu_+}, \quad (3b)$$

$$\varepsilon_1 \frac{\partial \varphi^{(1)}}{\partial \mu} \Big|_{-\mu_-} = \varepsilon_2 \frac{\partial \varphi^{(2)}}{\partial \mu} \Big|_{-\mu_-}, \quad (3c)$$

$$\varepsilon_1 \frac{\partial \varphi^{(1)}}{\partial \mu} \Big|_{\mu_+} = \varepsilon \frac{\partial \varphi^{(3)}}{\partial \mu} \Big|_{\mu_+}, \quad (3d)$$

where the last two equations are written after cancellation of the metric  $h_\mu$ -coefficients.



The appropriate product solutions of the Laplace's equations for the three regions in space can be written as follows:

$$\varphi_n^{(1)}(\mu, \eta) = (A_n e^{-n\mu} + B_n e^{n\mu}) \begin{cases} \cos(n\eta) \\ \sin(n\eta) \end{cases}, \quad (4a)$$

$$\varphi_n^{(2)}(\mu, \eta) = C_n e^{n\mu} \begin{cases} \cos(n\eta) \\ \sin(n\eta) \end{cases}, \quad (4b)$$

$$\varphi_n^{(3)}(\mu, \eta) = D_n e^{-n\mu} \begin{cases} \cos(n\eta) \\ \sin(n\eta) \end{cases}. \quad (4c)$$

These solutions satisfy the BC given by Eqs. (3a)-(3d) only for special values  $\varepsilon_n$  of  $\varepsilon$ , so that one can obtain the subsequent equations for  $A_n$  and  $B_n$ :

$$(\varepsilon_1 + \varepsilon_2) e^{n\mu_-} A_n - (\varepsilon_1 - \varepsilon_2) e^{-n\mu_-} B_n = 0, \quad (5a)$$

$$(\varepsilon_1 - \varepsilon_n) e^{-n\mu_+} A_n - (\varepsilon_1 + \varepsilon_n) e^{n\mu_+} B_n = 0. \quad (5b)$$

This set of homogeneous equations has nonzero solutions only if the determinant is null. This

gives rise to the following result:

$$\varepsilon_n = -\varepsilon_1 \frac{\varepsilon_1 \sinh [n (\mu_- + \mu_+)] + \varepsilon_2 \cosh [n (\mu_- + \mu_+)]}{\varepsilon_1 \cosh [n (\mu_- + \mu_+)] + \varepsilon_2 \sinh [n (\mu_- + \mu_+)]}, \quad (6)$$

consisting of a generalization for plasmon modes in two adjacent circular cross section nanorods derived by Mayergoyz [17].

Now consider that the cylinder of permittivity  $\varepsilon$  is located near a flat interface between media  $\varepsilon_1$  and  $\varepsilon_2$ . The solution for this configuration will be a particular case of the general result from Eq. (6). Transforming the cylinder with permittivity  $\varepsilon_2$  into a medium with a flat surface by setting  $\mu_- = 0$  and renaming  $\mu_+ \rightarrow \mu_c$  gives:

$$\varepsilon_n = -\varepsilon_1 \frac{(\varepsilon_1 + \varepsilon_2) e^{2n\mu_c} + (\varepsilon_2 - \varepsilon_1)}{(\varepsilon_1 + \varepsilon_2) e^{2n\mu_c} - (\varepsilon_2 - \varepsilon_1)}. \quad (7)$$

One can relate the parameter  $\mu_c$  to the cylinder's radius  $a$  and the distance  $d$  from its center to the interface through the following formula:

$$\mu_c = \operatorname{arccosh} (d/a). \quad (8)$$

Characterizing the cylinder by the dielectric function according to Drude model:

$$\varepsilon(\omega) = \varepsilon_\infty - \frac{\omega_p^2}{\omega^2}, \quad (9)$$

where  $\varepsilon(\omega)$  is the frequency-dependent relative permittivity,  $\varepsilon_\infty$  is the high-frequency dielectric constant and  $\omega_p$  is the plasma frequency, one obtains:

$$\omega_n = \omega_p \left[ \varepsilon_\infty + \varepsilon_1 \frac{(\varepsilon_1 + \varepsilon_2) e^{2n\mu_c} + (\varepsilon_2 - \varepsilon_1)}{(\varepsilon_1 + \varepsilon_2) e^{2n\mu_c} - (\varepsilon_2 - \varepsilon_1)} \right]^{-\frac{1}{2}}. \quad (10)$$

When the interface is absent, i.e.  $\varepsilon_1 = \varepsilon_2$ , Eq. (10) reduces to:

$$\omega_n = \omega_p (\varepsilon_\infty + \varepsilon_1)^{-\frac{1}{2}}. \quad (11)$$

Now consider that the cylinder and the lower half-space are made of the same material, so that  $\varepsilon_n = \varepsilon_2$ . For this special case one obtains a quadratic equation for  $\varepsilon_n$  in place of Eq. (7), which admits the following solutions:

$$\varepsilon_n^\pm = -\varepsilon_1 \frac{e^{n\mu_c} \pm 1}{e^{n\mu_c} \mp 1}. \quad (12)$$

The frequencies able to excite these modes can be written in terms of hyperbolic functions, thus reading:

$$\omega_n^+ = \omega_p \left[ \varepsilon_\infty + \varepsilon_1 \coth \left( \frac{n\mu_c}{2} \right) \right]^{-\frac{1}{2}} \quad (13a)$$

$$\omega_n^- = \omega_p \left[ \varepsilon_\infty + \varepsilon_1 \tanh \left( \frac{n\mu_c}{2} \right) \right]^{-\frac{1}{2}}. \quad (13b)$$

As  $\mu_c \geq 0$ , when the cylinder is far from the interface ( $d \gg a$ ), these relations also converge to Eq. (11). These oscillation modes correspond to the surface plasmons in free-space cylinders of circular cross section, as well as for configurations of infinite flat structures [17].

### 3. The Green's function for the two-dimensional Poisson's equation

#### 3.1. Electrostatic Green's function in two dimensions

In order to find a general solution for the electrostatic Poisson's equation with specific BC, we will use the Green's function method. Consider a potential  $\varphi(\mathbf{r})$  that satisfies the Poisson's equation in two dimensions in a medium characterized by the relative permittivity  $\varepsilon$ :

$$\nabla^2 \varphi(\mathbf{r}) = -\frac{\sigma(\mathbf{r})}{\varepsilon_0 \varepsilon}, \quad (14)$$

where  $\sigma(\mathbf{r})$  is the position-dependent surface charge density and  $\varepsilon_0$  is the vacuum permittivity. On the other hand, the potential at  $\mathbf{r} = (x, y)$  due to a point source at  $\mathbf{r}' = (x', y')$  is given by the Green's function (GF)  $G(\mathbf{r} - \mathbf{r}')$ , so that:

$$\nabla^2 G(\mathbf{r} - \mathbf{r}') = -\frac{\delta(\mathbf{r} - \mathbf{r}')}{\varepsilon}. \quad (15)$$

Note that in the expression above only the dimensionless relative permittivity  $\varepsilon$  enters the equation. Using Green's theorem it can be shown that  $\varphi(\mathbf{r})$  may be calculated through the knowledge of the source charge distribution and the GF:

$$\varphi(\mathbf{r}) = \frac{1}{\varepsilon_0} \int ds' \sigma(\mathbf{r}') G(\mathbf{r} - \mathbf{r}'). \quad (16)$$

The electrostatic GF in two dimensions for a medium characterized by the relative permittivity  $\varepsilon$  has the form:

$$G(\mathbf{r} - \mathbf{r}') = -\frac{1}{2\pi\varepsilon} \ln |\mathbf{r} - \mathbf{r}'|, \quad (17)$$

a result that can be obtained by solving explicitly the two-dimensional Poisson's equation. Another way of deriving this result is through the Fourier transform. Applying a partial Fourier transform along the  $x$ -direction to the Eq. (15) leads to:

$$\frac{\partial^2}{\partial y^2} G(q_x, y) - q_x^2 G(q_x, y) = -\frac{\delta(y)}{\varepsilon}. \quad (18)$$

This form of writing the GF assumes the possibility that  $y$ -direction is not translationally



invariant. Inserting the Fourier transforms in the  $y$ -coordinate in Eq. (18) and performing the inverse transform after this gives:

$$G(q_x, y) = \int_{-\infty}^{+\infty} \frac{dq}{2\pi\varepsilon} \frac{e^{iqy}}{(q - iq_x)(q + iq_x)} = G(-q_x, y) = \frac{e^{-|q_x||y|}}{2\varepsilon |q_x|}. \quad (19)$$

Making now the inverse transform in the  $q_x$ -coordinate, one obtains:

$$G(x, y) = \int_{-\infty}^{+\infty} \frac{dq_x}{2\pi} \cos(q_x x) \frac{e^{-|q_x||y|}}{2\varepsilon |q_x|}, \quad (20)$$

where the imaginary part vanished due to the limits of integration. The integral from Eq. (20) is formally divergent due to the logarithm behaviour at the origin. To compute it, we take its derivative in order to  $y$  and assume for now that  $y > 0$ . It is possible to show that:

$$\frac{\partial}{\partial y} G(x, y) = -\frac{1}{2\pi\varepsilon} \frac{y}{x^2 + y^2} \wedge y > 0. \quad (21)$$

Making the integration of the previous result over  $dy$ , we obtain the desired GF:

$$G(x, y) = -\frac{1}{2\pi\varepsilon} \ln \sqrt{x^2 + y^2} + C, \quad (22)$$

where the constant  $C$  (presumably infinite) can be dropped. For negative  $y$  one can repeat the recipe and obtain the same result, which is equivalent to Eq. (17).

In the case of a stratified medium, considering two half-spaces, the GF in an infinite space with dielectric function  $\varepsilon_j$  will be:

$$G_{jj}^\infty(q_x, y) = \frac{e^{-|q_x||y|}}{2\varepsilon_j |q_x|}. \quad (23)$$

In this case there will be four GFs, depending on which half-space the source and the observation point are in. If the source is in the  $j = 1$  half-space and the observation point in the same half-space or the one correspondent to  $j = 2$ , the two GFs will respectively read:

$$G_{11}(q_x, y, y') = \frac{e^{-|q_x||y-y'|}}{2\varepsilon_1 |q_x|} + Ae^{-|q_x|y}, \quad (24a)$$

$$G_{12}(q_x, y, y') = Be^{|q_x|y}. \quad (24b)$$

Applying the BC so that the source is at  $j = 1$  ( $y' > 0$ ), we obtain the following equations:

$$G_{11}(q_x, 0, y') = G_{12}(q_x, 0, y'), \quad (25a)$$

$$\varepsilon_1 \frac{\partial}{\partial y} G_{11}(q_x, y, y')|_{y=0} = \varepsilon_2 \frac{\partial}{\partial y} G_{12}(q_x, y, y')|_{y=0}. \quad (25b)$$

Equations (25a) and (25b) embody the continuity of both the electrostatic potential and of the electric displacement vector normal component. Solving the system of equations implied

by the BC and making the inverse Fourier transform, we finally obtain the total GFs of the structure:

$$\begin{aligned} G_{11}(\mathbf{r}, \mathbf{r}') &= -\frac{1}{2\pi\varepsilon_1} \ln |\mathbf{r} - \mathbf{r}'| - \frac{1}{2\pi\varepsilon_1} \frac{\varepsilon_1 - \varepsilon_2}{\varepsilon_1 + \varepsilon_2} \ln |\mathbf{r} - \tilde{\mathbf{r}}| = \\ &= \mathcal{G}(r, \theta, r', \theta') + \frac{\varepsilon_1 - \varepsilon_2}{\varepsilon_1 + \varepsilon_2} \mathcal{G}_d(r, \theta, r', \theta'), \end{aligned} \quad (26a)$$

$$G_{12}(\mathbf{r}, \mathbf{r}') = -\frac{1}{2\pi\varepsilon_1} \frac{2\varepsilon_1}{\varepsilon_1 + \varepsilon_2} \ln |\mathbf{r} - \mathbf{r}'|, \quad (26b)$$

where  $\tilde{\mathbf{r}} = (x', -y')$ . Note that the 2D electrostatic GF does not vanish at infinity. Using the same procedure one can compute  $G_{22}$  and  $G_{21}$ , which correspond to the situation when the source is in the half-space  $j = 2$ .

If the cylinder is located at the origin and the interface between the two media lies at  $y = -d$  (Fig. 1), performing the same procedure as before gives rise to  $G_{11}(\mathbf{r}, \mathbf{r}')$  and  $G_{12}(\mathbf{r}, \mathbf{r}')$  with the same form as given by Eqs. (26a) and (26b), but with  $\tilde{\mathbf{r}} = (x', -y' - 2d)$ . The absolute value of the new  $\tilde{\mathbf{r}}$  reads:

$$|\tilde{\mathbf{r}}| = \sqrt{(x')^2 + (y' + 2d)^2} = \sqrt{(r')^2 + 4dr' \sin \theta' + 4d^2}, \quad (27)$$

where the relation to polar coordinates is  $x' = r' \cos \theta'$  and  $y' = r' \sin \theta'$ .

#### 4. Determination of the fields in the composite system: Eycles' method

Now that the desired Green's function is determined, we can find the electrostatic potential everywhere from the knowledge of what happens on the surface of the cylinder. The total potential acting on the rod is the sum of the external potential  $\varphi_{ext}(\mathbf{r})$  with the one created by the polarization charges,  $\varphi_\sigma(\mathbf{r})$ :

$$\varphi(\mathbf{r}) = \varphi_{ext}(\mathbf{r}) + \varphi_\sigma(\mathbf{r}). \quad (28)$$

The dipole moment per unit volume is the 3D polarization  $\mathbf{P}(\mathbf{r}')$ , where  $\mathbf{r}'$  is the position vector right below the contour line limiting the cross section of the cylinder. The induced charge density per unit area ( $\sigma$ ) is related to  $\mathbf{P}$  as:

$$\sigma(\mathbf{r}') = \hat{\mathbf{n}}' \cdot \mathbf{P}(\mathbf{r}'), \quad (29)$$

where  $\hat{\mathbf{n}}'$  is a unit vector perpendicular to the surface of the cylinder. The potential due to the new charge density is calculated through Eq. (16). The total field is given by  $\mathbf{E} = -\nabla\varphi(\mathbf{r})$  and the polarization is related to the aforementioned via the electric susceptibility, defined

as  $\chi = \varepsilon - 1$ , according to:

$$\mathbf{P}(\mathbf{r}') = \varepsilon_0 \chi \mathbf{E} = -\varepsilon_0 \chi \nabla' \varphi(\mathbf{r}'). \quad (30)$$

Using these definitions and Eq. (16), the total potential reads:

$$\varphi(\mathbf{r}) = \varphi_{ext}(\mathbf{r}) - \chi \int_s ds \hat{\mathbf{n}}' \cdot \nabla' \varphi(\mathbf{r}') G(\mathbf{r} - \mathbf{r}'), \quad (31)$$

where the integral is over the contour line limiting the cross section of the cylinder. We can see that the integral equation (31), firstly proposed by Eyges [18], allows to compute the potential everywhere in space when a uniform body of arbitrary shape is placed in an external electrostatic field.

The first thing to do is to determine the potential on the cylinder's surface. With the rod in the upper half-space (Fig. 1), we have to solve the following equation:

$$\varphi(a, \theta) = \varphi_{ext}(a, \theta) - \chi \int_s ds \hat{\mathbf{n}}' \cdot \nabla' \varphi(\mathbf{r}')|_{r'=a} G_{11}(a, \theta, a, \theta'). \quad (32)$$

For the potential inside the cylinder,  $\varphi_{in}(r, \theta)$ , one can write the following expansion:

$$\varphi_{in}(r, \theta) = \sum_{l=-\infty}^{+\infty} c_l \left(\frac{r}{a}\right)^{|l|} e^{il\theta}, \quad r < a. \quad (33)$$

To determine the coefficients  $c_l$ , we write Eq. (32) for each index  $l$  and expand  $\varphi_{in}(a, \theta)$  according to Eq. (33) on both sides. As the number of coefficients is infinite, the system has to be truncated at some  $|l| = l_{\max}$ , so that there will be  $2l_{\max} + 1$  equations to solve, each with the same number of terms on the right-hand side. Multiplying by  $e^{-il\theta}$  and integrating over  $\theta$  from 0 to  $2\pi$  gives:

$$2\pi c_l = \int_0^{2\pi} d\theta \varphi_{ext}(a, \theta) e^{-il\theta} - \chi \sum_{\substack{m=-l_{\max} \\ m \neq 0}}^{l_{\max}} |m| c_m \int_0^{2\pi} \int_0^{2\pi} d\theta' d\theta G_{11}(a, \theta, a, \theta') e^{-i(l\theta - m\theta')}. \quad (34)$$

According to Eq. (24a), for a cylinder in free space only the  $\mathcal{G}$  part of  $G_{11}(a, \theta, a, \theta')$  enters the system above, so writing the logarithm argument in polar coordinates, we have to perform the following integration:

$$I_{\mathcal{G}} = \int_0^{2\pi} \int_0^{2\pi} d\theta' d\theta \ln \left[ a^2 (\cos \theta - \cos \theta')^2 + a^2 (\sin \theta - \sin \theta')^2 \right] e^{-i(l\theta - m\theta')}. \quad (35)$$

One can show that all the terms of the integral above with  $l \neq m$  vanish. For  $l = m \in \{0, \pm 1\}$  it can be computed analytically, while the general solution for any  $l = m$  was obtained by

intuition and numerically confirmed, thus reading:

$$I_G = \begin{cases} -\frac{4\pi^2}{|m|}, & l = m \neq 0, \\ 8\pi^2 \ln a, & l = m = 0, \\ 0, & l \neq m. \end{cases} \quad (36)$$

Note that  $8\pi^2 \ln a$  is always multiplied by zero due to the presence of  $|m|$  in Eq. (34), so that only the  $\mathcal{G}(a, \theta, a, \theta')$  terms with  $l = m \neq 0$  contribute for the potentials. The determination of coefficients  $c_l$  becomes nontrivial when one has to take the interface into account. For the Green's function interface part,  $\mathcal{G}_d(a, \theta, a, \theta')$ , the  $y$ -coordinate of the source is  $-y' - 2d$ , so the integral to compute reads:

$$I_{G_d} = \int_0^{2\pi} \int_0^{2\pi} d\theta' d\theta \ln \left[ a^2 (\cos \theta - \cos \theta')^2 + a^2 \left( \sin \theta + \sin \theta' + \frac{2d}{a} \right)^2 \right] e^{-i(l\theta - m\theta')}. \quad (37)$$

Performing numerical integration for different ratios  $d/a$ , we were able to find empirically an analytical result for the previous integral, valid for  $d \geq a$ :

$$I_{G_d} = \begin{cases} -i^{(l-m)} \frac{4\pi^2 (|l| + |m| - 1)!}{|m| |l|! (|m| - 1)!} \left( \frac{a}{2d} \right)^{|l|+|m|}, & l \cdot m > 0, \\ -i^l \frac{4\pi^2}{|l|} \left( \frac{a}{2d} \right)^{|l|}, & m = 0, l \neq 0, \\ -i^{-m} \frac{4\pi^2}{|m|} \left( \frac{a}{2d} \right)^{|m|}, & l = 0, m \neq 0, \\ 8\pi^2 \ln(2d), & l = m = 0, \\ 0, & l \cdot m < 0. \end{cases} \quad (38)$$

The solutions of the integrals  $I_G$  and  $I_{G_d}$  presented above allow to make several conclusions about the linear system given by Eq. (34). The  $\mathcal{G}(a, \theta, a, \theta')$  part of the GF only contributes for terms with  $l = m$ , the diagonal ones. On the other hand,  $\mathcal{G}_d(a, \theta, a, \theta')$  gives rise to diagonal terms, which can be written in terms of Catalan numbers, and also to non-diagonal ones when  $l$  and  $m$  are of the same sign. For each  $l$  the term with  $m = 0$  is multiplied by zero according to Eq. (34), what makes the equation for  $c_0$  linearly independent from the others. This way one can write the following expression for  $c_0$ :

$$c_0 = -\frac{\chi}{2\varepsilon_1} \frac{\varepsilon_1 - \varepsilon_2}{\varepsilon_1 + \varepsilon_2} \sum_{\substack{m=-l_{\max} \\ m \neq 0}}^{l_{\max}} i^{-m} \left( \frac{a}{2d} \right)^{|m|} c_m. \quad (39)$$

For all the other  $c$ -coefficients the set given by Eq. (34) can be written in matrix form as:

$$\begin{bmatrix} \vdots \\ c_{-2} \\ c_{-1} \\ c_1 \\ c_2 \\ \vdots \end{bmatrix} = \begin{bmatrix} \vdots \\ 0 \\ I_{-1}^{ext} \\ I_1^{ext} \\ 0 \\ \vdots \end{bmatrix} + \begin{bmatrix} \ddots & \vdots & \vdots & \vdots & \vdots & \ddots \\ \cdots & \mathbb{G}_{-2-2} & \mathbb{G}_{-2-1} & 0 & 0 & \cdots \\ \cdots & \mathbb{G}_{-1-2} & \mathbb{G}_{-1-1} & 0 & 0 & \cdots \\ \cdots & 0 & 0 & \mathbb{G}_{11} & \mathbb{G}_{12} & \cdots \\ \cdots & 0 & 0 & \mathbb{G}_{21} & \mathbb{G}_{22} & \cdots \\ \ddots & \vdots & \vdots & \vdots & \vdots & \ddots \end{bmatrix} \begin{bmatrix} \vdots \\ c_{-2} \\ c_{-1} \\ c_1 \\ c_2 \\ \vdots \end{bmatrix}, \quad (40)$$

where the non-null matrix elements  $\mathbb{G}_{lm}$  read:

$$\mathbb{G}_{lm} = -\frac{\chi}{2\varepsilon_1} \left[ \delta_{lm} + i^{(l-m)} \frac{\varepsilon_1 - \varepsilon_2}{\varepsilon_1 + \varepsilon_2} \frac{(|l| + |m| - 1)!}{|l|! (|m| - 1)!} \left( \frac{a}{2d} \right)^{|l|+|m|} \right], \quad l \cdot m > 0, \quad (41)$$

while the non-homogeneous terms are given by:

$$I_l^{ext} = \frac{1}{2\pi} \int_0^{2\pi} d\theta \varphi_{ext}(a, \theta) e^{-il\theta}, \quad l = \pm 1. \quad (42)$$

The matrix from Eq. (40) can be divided into two blocks, making its solution simpler. After obtaining the  $c$ -coefficients, the potential inside can be written through Eq. (33), taking  $c_0$  into account. The potential outside the cylinder can be determined through the following expression:

$$\varphi_{out}(\mathbf{r}) = \varphi_{ext}(\mathbf{r}) - \chi \sum_{\substack{m=-l_{\max} \\ m \neq 0}}^{l_{\max}} |m| c_m \int_0^{2\pi} d\theta' e^{im\theta'} G(r, \theta, a, \theta'), \quad (43)$$

where for the case of configuration from Fig. 1 the GF will be one of the following:

$$G_{11}(r, \theta, a, \theta') = -\frac{1}{4\pi\varepsilon_1} \ln \left[ (r \cos \theta - a \cos \theta')^2 + (r \sin \theta - a \sin \theta')^2 \right] - \frac{1}{4\pi\varepsilon_1} \frac{\varepsilon_1 - \varepsilon_2}{\varepsilon_1 + \varepsilon_2} \ln \left[ (r \cos \theta - a \cos \theta')^2 + (r \sin \theta + a \sin \theta' + 2d)^2 \right], \quad (44a)$$

$$G_{12}(r, \theta, a, \theta') = -\frac{1}{4\pi\varepsilon_1} \frac{2\varepsilon_1}{\varepsilon_1 + \varepsilon_2} \ln \left[ (r \cos \theta - a \cos \theta')^2 + (r \sin \theta - a \sin \theta')^2 \right]. \quad (44b)$$

We note here that the terms

$$r = \frac{\varepsilon_1 - \varepsilon_2}{\varepsilon_1 + \varepsilon_2}, \quad t = \frac{2\varepsilon_1}{\varepsilon_1 + \varepsilon_2} \quad (45)$$

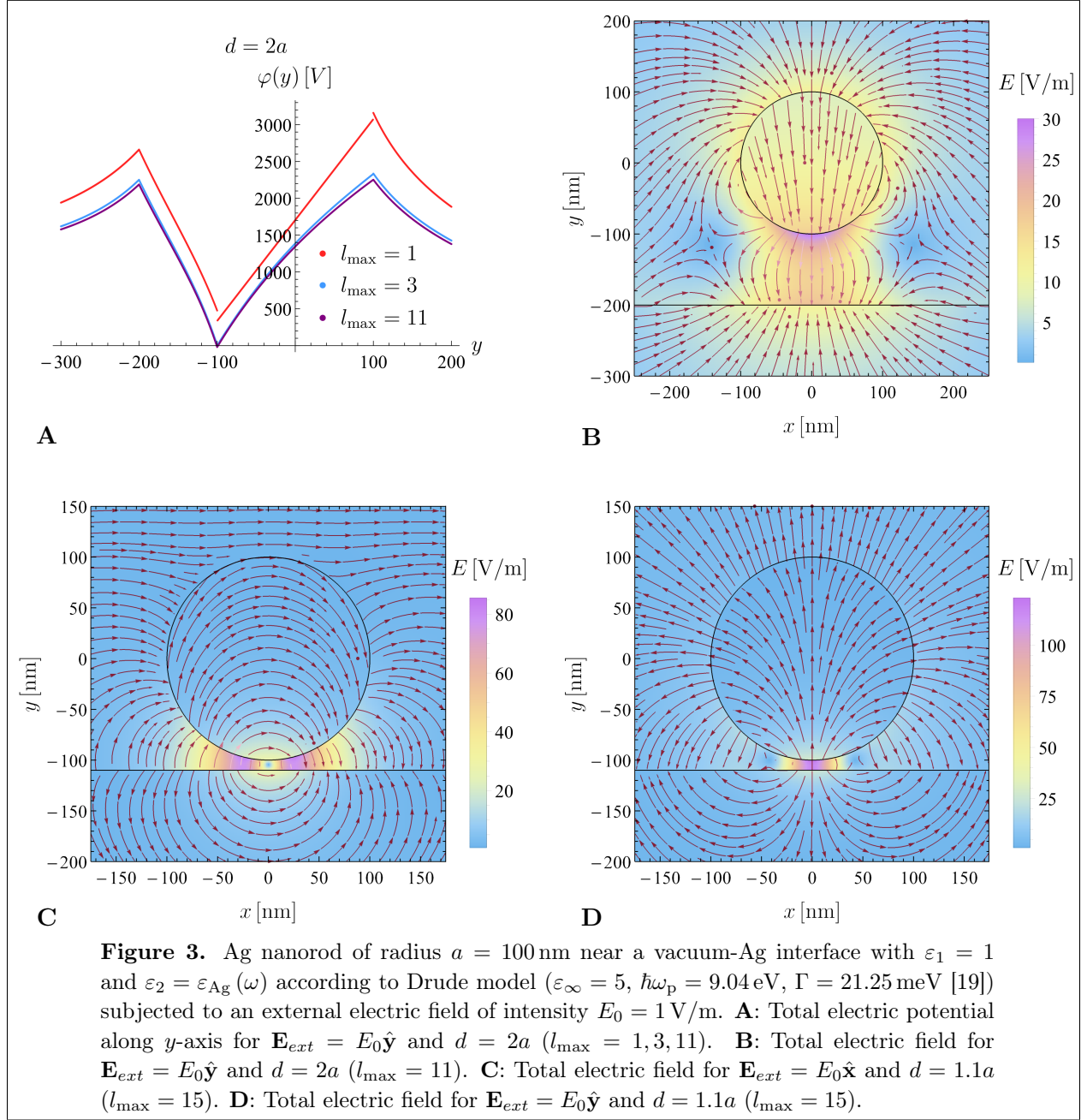
are respectively the Fresnel reflection and transmission coefficients of an electromagnetic wave with normal incidence on an interface in the electrostatic limit. The integration over  $\theta'$  in Eq. (43) with  $G_{11}(r, \theta, a, \theta')$  will determine the potential above the interface, while using  $G_{12}(r, \theta, a, \theta')$  one will obtain what happens to the potential in the substrate.

Solving the problem with  $l_{\max} = 1$  for  $d = 2a$  and  $\varphi_{ext} = -E_0 r \sin \theta$ , by fixing  $\theta = \pi/2$  one is able to write the following result:

$$\varphi\left(r, \frac{\pi}{2}\right) = \begin{cases} \varphi_{in} = i\left(\pm\frac{2r}{a} + \frac{\chi}{4\varepsilon_1}\frac{\varepsilon_1 - \varepsilon_2}{\varepsilon_1 + \varepsilon_2}\right)c_1, & r < a, \\ \varphi_{out} = -i\frac{\chi}{\varepsilon_1}\left(\pm\frac{a}{r} - \frac{\varepsilon_1 - \varepsilon_2}{\varepsilon_1 + \varepsilon_2}\frac{1}{4\pm r/a}\right)c_1 \mp E_0 r, & r > a, \quad y > 0, \\ \varphi_{out} = -i\frac{\chi}{\varepsilon_1}\frac{2\varepsilon_1}{\varepsilon_1 + \varepsilon_2}\frac{a}{r}c_1 + E_0 r, & y < -d, \end{cases} \quad (46)$$

where the sign of  $r$  in  $\varphi_{in}$  and  $\varphi_{out}$  is positive if  $y > 0$  and negative for  $y < 0$ , while the coefficient  $c_1$  reads:

$$c_1 = \frac{iE_0 a}{2 + \frac{\chi}{\varepsilon_1}\left(1 + \frac{1}{16}\frac{\varepsilon_1 - \varepsilon_2}{\varepsilon_1 + \varepsilon_2}\right)}. \quad (47)$$



The  $c$ -coefficients and hence the potential inside the cylinder can be obtained analytically. The general result for the potential outside the cylinder can be calculated numerically, allowing to determine the electric field everywhere through  $\mathbf{E} = -\nabla\varphi_{\text{out}}(\mathbf{r})$ . Plotting the total potential along the  $y$ -axis for the case of an Ag nanorod at a distance  $d = 2a$  from a vacuum-Ag interface (Fig. 3A), it is possible to see that with  $l_{\text{max}} = 1$  the potential is slightly discontinuous across the nanorod's surface, but converges very quickly to a continuous

solution, and at  $l_{\max} = 3$  it almost overlaps the solution with  $l_{\max} = 11$ . When the cylinder is closer to the surface, the convergence is slower and higher  $l_{\max}$  is needed to solve the problem correctly. Different field patterns are obtained depending on the distance  $d$  and also on the direction of  $\mathbf{E}_{ext}$ . Inside the nanorod the field lines follow the direction of the external electric field for  $l_{\max} = 1$ , but become progressively distorted by the scattered potential as one takes more higher-order terms into account. When  $\mathbf{E}_{ext}$  is perpendicular to the media border (Figs. 3B and 3D), the maximal field magnitude occurs exactly in the middle of the gap between the rod and the interface. In this region the stream lines converge (Fig. 3B) or diverge (Fig. 3D) from the flat surface, depending on the distance the cylinder is located from the substrate. This corresponds respectively to accumulation of negative or positive charge on the area just below the cylinder. One can also see that the closer the nanorod is to the substrate, the higher is the magnitude of the field in the gap between the two. If  $\mathbf{E}_{ext}$  has parallel incidence (Fig. 3C), then there are two regions where the intensity of the electric field is higher, each with different sign, having lower magnitude comparatively to the perpendicular incidence.

#### 4.1. Polarizability of the nanorod

Using the relation between the polarization  $\mathbf{P}$  and the electric field  $\mathbf{E}$  from Eq. (30), we can write for the dipole moment  $\mathbf{p}$ :

$$\mathbf{p} = \int_V dV \mathbf{P} = -\varepsilon_0 \chi \int dV \nabla' \varphi(\mathbf{r}'), \quad (48)$$

what can be transformed into a surface integral using the divergence theorem:

$$\mathbf{p} = -\varepsilon_0 \chi \int ds \hat{\mathbf{n}}' \varphi(\mathbf{r}'). \quad (49)$$

Expressing the total potential through Eq. (33) and writing  $\hat{\mathbf{n}}' = \hat{\mathbf{r}}' = (\cos \theta, \sin \theta)$  we obtain:

$$\begin{aligned} \mathbf{p} &= -\varepsilon_0 \chi a \sum_{l=-\infty}^{+\infty} c_l \int_0^{2\pi} d\theta e^{il\theta} (\cos \theta, \sin \theta) = \\ &= -\varepsilon_0 \chi a \pi [c_{-1} + c_1, -i(c_{-1} - c_1)]. \end{aligned} \quad (50)$$

Since the polarizability  $\alpha$  satisfies the relation  $\mathbf{p} = \alpha \mathbf{E}_0$ , having in mind that the  $c$ -coefficients contain the factor  $aE_0$ , the diagonal components of the polarizability tensor read:

$$\alpha_{xx} = -\frac{\varepsilon_0 \chi a}{E_0} \pi (c_{-1} + c_1), \quad (51a)$$



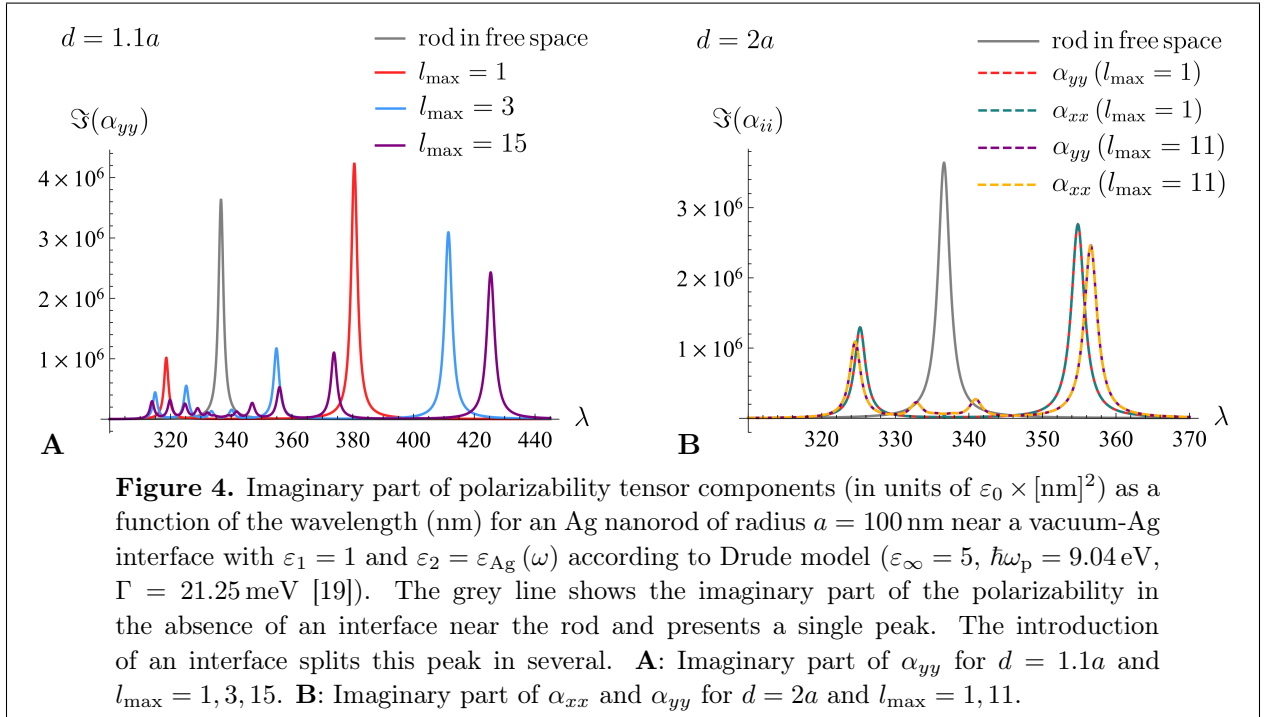
$$\alpha_{yy} = i \frac{\varepsilon_0 \chi a}{E_0} \pi (c_{-1} - c_1). \quad (51b)$$

For external field with normal incidence the coefficients  $c_1$  and  $c_{-1}$  have the same absolute value and opposite sign, being the first given by Eq. (47) for  $l_{\max} = 1$  and  $d = 2a$ , so that only  $\alpha_{yy}$  exists. For parallel incidence the coefficients  $c_{\pm 1}$  are equal, hence only  $\alpha_{xx}$  does not vanish. Note that contrary to a finite three-dimensional body, the polarizability of the infinite cylinder has units of  $\varepsilon_0 \times \text{Area}$  instead of  $\varepsilon_0 \times \text{Volume}$ .

The polarizability tensor components depend on the distance  $d$ , which is also hidden in the  $c$ -coefficients. Plots of the imaginary part of the diagonal components of  $\alpha_{ij}$  (Fig. 4) show that the smaller the distance  $d$ , the longer it takes for the sum of the modes to converge. On Fig. 4B we can also see that  $\alpha_{xx}$  and  $\alpha_{yy}$  coincide, expressing the isotropy of the polarizability. The position of the relative maxima of  $\Im(\alpha_{ii})$  is exactly predicted by the solution of Laplace's equation with appropriate BC performed in Section 2. The wavelengths of the natural modes are given by:

$$\lambda_n^\pm = \lambda_p \sqrt{\varepsilon_\infty + \varepsilon_1 \frac{e^{n\mu_c} \pm 1}{e^{n\mu_c} \mp 1}}, \quad (52)$$

where  $\lambda_p$  is the wavelength correspondent to the classical plasma frequency and  $\mu_c = \text{arccosh}(d/a)$ . For  $d = 1.1a$  the peaks at 313.9 nm and 425.4 nm correspond respectively



to  $\lambda_1^-$  and  $\lambda_1^+$ , the maxima at 319.8 nm and 373.8 nm respectively to  $\lambda_2^-$  and  $\lambda_2^+$  and so on. Note that it is necessary to use larger values of  $l_{\max}$  to obtain the precise position of the maxima for  $d = 1.1a$  correspondent to  $\lambda_5^\pm$ , for example, as the modes with higher  $n$  take longer to converge. When  $n \rightarrow \infty$ , the geometrical factor  $(e^{n\mu_c} \pm 1) / (e^{n\mu_c} \mp 1)$  tends to 1, so for any ratio  $d/a$  the wavelengths of the peaks will converge to:

$$\lambda = \lambda_p \sqrt{\varepsilon_\infty + \varepsilon_1}, \quad (53)$$

what corresponds to the natural frequency of plasmon modes in cylinders of circular cross section and in infinite flat structures [17].

One can use the imaginary part of the polarizability tensor components to calculate the extinction cross section. The last one is defined as the sum of the absorption and scattering cross sections and can be written as:

$$\sigma_{ex} = \sigma_{ab} + \sigma_{sc} = \frac{k}{\varepsilon_0} \Im(\alpha_{ii}), \quad (54)$$

where  $k = \omega/c$ . We note here that the extension of the cross section in two dimensions has units of length and not of area, as in three-dimensional problems.

## 5. Conclusions and outlook

In this paper we have studied analytically a plasmonic system composed of a nanorod in the vicinity of a plasmonic metallic surface, forming a small gap between both structures. The study was performed in the electrostatic and local approximations. The first approximation is accurate in the regime  $\lambda \gg a$ , where  $a$  is the rod's radius, so that retardation plays no significant role. The second approximation is justifiable as long as the gap between the rod and metallic plane is not too small. The inclusion of nonlocal effects [20] poses considerably additional difficulties to the calculations because an extra field component and an additional boundary condition appear [21]. However, for distances of the order of a few nanometers or smaller, nonlocal effects rise in importance and prevent the evergrowing enhancement of field intensity as the gap between the nanostructure and the semi-infinite plane is reduced. Additionally, for very narrow gaps quantum effects start to play an important role and we enter the realm of quantum plasmonics. Having an analytical description of both nonlocal and quantum effects is the goal of a future publication. The inclusion of two-dimensional materials in the system considered in this paper is an extension worth pursuing due to the recent demonstration of extraordinary confinement of graphene acoustic plasmons in metallic

nanostructures of the form considered here [22]. The original experiments in the hybrid system composed of graphene and nanocubes showed extraordinary field enhancement and confinement. The same is expected if nanorods are deposited on top of graphene instead of nanocubes. The nanorod, however, represents considerable interest itself, since the shape of the field will be different, which may open an additional degree of freedom when it comes to the application of this type of hybrid system for molecular sensing in the mid-IR. The extension of this work to include 2D materials, at the lowest level of approximation, is relatively simple. The main new complication comes from the new form of one of the boundary conditions, where the derivatives normal to 2D materials are now discontinuous, due to the charge density accumulated, for example, in graphene. The integrals in Eyges' method become, however, more complicated.

## **Acknowledgments**

N.M.R.P. thanks André Gonçalves and Bruno Amorim for many discussions on the topic of plasmonics. N.M.R.P. acknowledges support by the Portuguese Foundation for Science and Technology (FCT) in the framework of the Strategic Funding UIDB/04650/2020, support from the European Commission through the project “Graphene-Driven Revolutions in ICT and Beyond” (Ref. No. 881603, CORE 3), COMPETE 2020, PORTUGAL 2020, FEDER and the FCT through projects POCI-01-0145-FEDER-028114.

- [1] Monticone F and Alù A 2017 *Reports on Progress in Physics* **80** 036401
- [2] Stockman M I, Kneipp K, Bozhevolnyi S I, Saha S, Dutta A, Ndukaife J, Kinsey N, Reddy H, Guler U, Shalaev V M, Boltasseva A, Gholipour B, Krishnamoorthy H N S, MacDonald K F, Soci C, Zheludev N I, Savinov V, Singh R, Groß P, Lienau C, Vadai M, Solomon M L, Barton D R, Lawrence M, Dionne J A, Boriskina S V, Esteban R, Aizpurua J, Zhang X, Yang S, Wang D, Wang W, Odom T W, Accanto N, de Roque P M, Hancu I M, Piatkowski L, van Hulst N F and Kling M F 2018 *Journal of Optics* **20** 043001
- [3] Klimov V V 2013 *Nanoplasmonics* (Boca Raton: CRC Press) ISBN 9789814267168
- [4] Pelton B 2013 *Plasmonics* (John Wiley & Sons) ISBN 1118060407
- [5] Maier S A 2007 *Plasmonics* (Springer-Verlag GmbH) ISBN 0387331506
- [6] Sun Y, Su Y, Dai Z and Wang W 2014 *Journal of Optics* **16** 055003
- [7] Moreau A, Ciraci C, Mock J J, Hill R T, Wang Q, Wiley B J, Chilkoti A and Smith D R 2012 *Nature* **492** 86–89
- [8] Kildishev A V, Boltasseva A and Shalaev V M 2013 *Science* **339** 1232009–1232009
- [9] Olaimat M M, Yousefi L and Ramahi O M 2021 *Journal of the Optical Society of America B* **38** 638
- [10] Jung J and Pedersen T G 2012 *Optics Express* **20** 3663
- [11] Schieber D 1999 *Journal of Electrostatics* **48** 65–75
- [12] Lekner J 2013 *Journal of Electrostatics* **71** 1104–1110
- [13] Venermo J and Sihvola A 2005 *Journal of Electrostatics* **63** 101–117
- [14] Phillips H B 1934 *Journal of Mathematics and Physics* **13** 261–267
- [15] Kellogg O D 1967 *Foundations of Potential Theory* (Springer Berlin Heidelberg)
- [16] Dhondt G and Köhl M 1997 *Quarterly of Applied Mathematics*
- [17] Mayergoyz I D 2012 *Plasmon Resonances in Nanoparticles* (World Scientific Publishing Company) ISBN 9814350656
- [18] Eyges L 1975 *Annals of Physics* **90** 266–282
- [19] Zeman E J and Schatz G C 1987 *The Journal of Physical Chemistry* **91** 634–643
- [20] Hildebrandt A, Blossey R, Rjasanow S, Kohlbacher O and Lenhof H P 2004 *Physical Review Letters* **93** 108104
- [21] Gonçalves P A D, Christensen T, Peres N M R, Jauho A P, Epstein I, Koppens F H L, Soljačić M and Mortensen N A 2021 *Nature Communications* **12** 3271
- [22] Epstein I, Alcaraz D, Huang Z, Pusapati V V, Hugonin J P, Kumar A, Deputy X M, Khodkov T, Rappoport T G, Hong J Y, Peres N M R, Kong J, Smith D R and Koppens F H L 2020 *Science* **368** 1219–1223